Crystallization and Preliminary Structure Determination of Porcine Aldehyde Reductase from Two Crystal Forms

By Ossama El-Kabbani, Guangda Lin, Sthanam V. L. Narayana and Karen M. Moore

The University of Alabama at Birmingham, Center for Macromolecular Crystallography, Box 79-HT, Birmingham, Alabama 35294-0005, USA

Nancy C. Green and T. G. Flynn

Department of Biochemistry, Queen's University, Kingston, Ontario, Canada, K7L 3N6

and Lawrence J. DeLucas

The University of Alabama at Birmingham, Center for Macromolecular Crystallography, Box 79-HT, Birmingham, Alabama 35294-0005, USA

Abstract

Aldehyde reductase from porcine kidney has been crystallized from buffered ammonium sulfate solutions. Two crystal forms are monoclinic, space group $P2_1$, with $a = 56.2$, $b = 98.1$, $c = 73.2$ Å, $\beta = 112.5°$ and $a = 92.4$, $b = 62.1$, $c = 59.0$ Å, $\beta = 94.6°$. A third crystal form is hexagonal with $a = b = 166.0$, $c = 66.0$ Å, $\alpha = \beta = 90.0°$ and $\gamma = 120.0°$. Molecular-replacement structure solutions have been successfully obtained for the two monoclinic crystal forms. The crystallographic R factor at 8–2.8 Å resolution for the two monoclinic crystal forms is currently 0.23 and 0.25, respectively. There are two molecules per asymmetric unit related by a non-crystallographic twofold axis. The aldehyde reductase models are supported by the arrangement of the molecules in their respective unit cells and by electron densities corresponding to amino-acid side chains not included in the search structures.

Introduction

Aldehyde reductase from pig kidney belongs to a large family of widely distributed monomeric NADPH-dependent oxidoreductases. These enzymes catalyze the reduction of a wide range of aliphatic and aromatic aldehydes to their corresponding alcohols (Flynn, 1982). The predominant enzyme in many mammalian tissues, particularly in the liver, brain and kidney, is a tissue-specific aldehyde reductase (*e.g.* pig kidney aldehyde reductase). The other major enzyme, aldose reductase, has been identified in muscle and lens in addition to other mammalian tissues. Both enzymes share several physical and chemical properties including overlapping substrate specificities and similar co-factor requirements (Cromlish & Flynn, 1983; Markus, Raducha & Harris, 1983; Kubiseski, Hyndman, Morjana & Flynn, 1992). The three-dimensional structure of porcine aldose reductase has been determined by this laboratory at low resolution (unpublished results) and at 2.5 Å resolution by Rondeau *et al.* (1992). The human aldose reductase structure has been determined by 1.65 Å by Wilson, Bohren, Gabbay & Quiocho (1992). Since the sequences of aldose and aldehyde reductases are highly homologous (Bohren, Bullock, Wermuth & Gabbay, 1989) their three-dimensional structures should be similar.

Recent evidence suggests that aldose reductase is responsible for diabetic complications in the eye and other major organs (Kinoshita & Nishimura, 1988). Aldose reductase is almost totally confined to the medulla of the kidney, but diabetic complications arise in the cortex. It has been postulated that because of the high concentration of aldehyde reductase in the renal cortex, over an extended period of time this concentration might be sufficient to result in significant accumulation of sorbitol despite the enzyme's poor activity with respect to glucose. Under these conditions, inhibiting both enzymes is the most efficient way to prevent the complications of diabetes. A major problem with all inhibitors developed to date for aldose reductase and aldehyde reductase is that they are either non-competitive or uncompetitive inhibitors (Stribling, Mirlees, Harrison & Earl, 1986) and are thus not directed at the active site.

The structure determination of aldehyde reductase will be extremely valuable for several reasons: (1) Since the amino acids involved in the co-factor binding site for aldose and aldehyde reductase are highly

conserved, knowledge of the exact configuration and geometry of these amino acids will provide valuable information for the design of inhibitors that are specific for aldose and/or aldehyde reductase. (2) Aldose reductase binds NADPH and NADH while aldehyde reductase binds only NADPH. Knowledge of the exact geometry of the amino acids at the active site for aldehyde reductase will help explain the mechanism of action with co-factor and substrate. (3) Knowledge of the overall three-dimensional structure of aldehyde reductase may provide insight as to possible non-competitive sites that may be useful targets for drug design. In relation to the above studies, we have purified porcine kidney aldehyde reductase to apparent homogeneity, crystallized the enzyme by the vapor-diffusion technique using ammonium sulfate as a precipitant, and obtained a structure solution for two crystal forms using a combination of molecular-replacement and single isomorphous replacement techniques.

Experimental

Crystallization and data collection

Porcine kidney aldehyde reductase was purified from fresh pig kidneys by a modification of the method of Cromlish & Flynn (1983). The two critical modifications to the published method were carrying out the purification in a TRIS buffer system instead of sodium phosphate, and the inclusion of size-exclusion high-performance liquid chromatography as the final step. A detailed description of the purification procedure will appear elsewhere. Monoclinic and hexagonal crystals of the apo-enzyme were grown at 295 and 277 K, respectively, by vapor diffusion using the hanging-drop method (McPherson, 1985). 2 μl droplets of protein (12 mg ml^{-1}), previously dialyzed against 10 mM PIPES buffer with 2 mM 2-mercaptoethanol, pH 6.2, were mixed with 2 μl of a 20% ammonium sulfate solution in 10 mM PIPES, 2 mM 2-mercaptoethanol, pH 6.5 and 2 μl of a 10 mM β-octylglucoside solution in 10 mM PIPES, 2 mM 2-mercaptoethanol, pH 6.5. The droplets were vapor equilibrated against 1 ml of a 35% ammonium sulfate solution in 50 mM PIPES, 2 mM 2-mercaptoethanol, pH 6.5. The temperature was the only difference between the crystallization conditions of the monoclinic and hexagonal crystals.

The monoclinic crystals diffract strongly to 2.4 Å resolution and are stable for more than 120 h in Cu $K\alpha$ radiation (40 kV, 100 mA) generated by a fine-focus rotating-anode generator (RU-200, Rigaku). The hexagonal crystals diffract up to 4.5 Å resolution and are stable in the beam for approximately 50 h. X-ray diffraction data from one native monoclinic aldehyde reductase crystal were recorded

on a Nicolet multiwire area detector and processed by the *XENGEN* program package (Howard *et al.*, 1987). The space group is $P2_1$, with $a = 56.2$, $b = 98.1$, $c = 73.2$ Å, $\alpha = 90.0$, $\beta = 112.5$, $\gamma = 90.0°$. The final native data had 15 830 out of 18 032 possible unique reflections with 12 090 reflections measured more than once within the 2.8 Å resolution sphere. The value for R_{sym} is equal to 10.7% and the overall mean ratio of I to $\sigma(I)$ is equal to 17.1 for the 2.8 Å resolution data set. R_{sym} is defined as $\sum_{hkl}\sum_i^N|\bar{I} - I_i|/\sum_{hkl}N\bar{I}$, where $\bar{I}$ is the mean intensity of the N reflections with intensities I_i and common indices h,k,l. A self-rotation-function solution was obtained using the *MERLOT* package (Fitzgerald, 1988). The self-rotation function was calculated using data between 12 and 5 Å resolution, with a cut-off radius of 29.9 Å. A peak of 2.4 standard deviations above background was displayed at $\psi = 90.0$, $\varphi = 22.0$ and $\kappa = 180.0°$ indicating that there are two molecules per asymmetric unit related by a non-crystallographic twofold axis (Fig. 1).

More recently, a new monoclinic crystal form was also obtained at 295 K under exactly the same crystallization conditions. The crystals belong to the space group $P2_1$, with $a = 92.4$, $b = 62.1$, $c = 59.0$ Å, $\alpha = 90.0$, $\beta = 94.6$, $\gamma = 90.0°$. X-ray diffraction data using two native aldehyde reductase crystals were collected and the final merged data (resolution 2.53 Å) had 19 357 out of 22 591 possible unique reflections with 15 646 reflections measured more than once. The value for R_{sym} is 10.2% and the
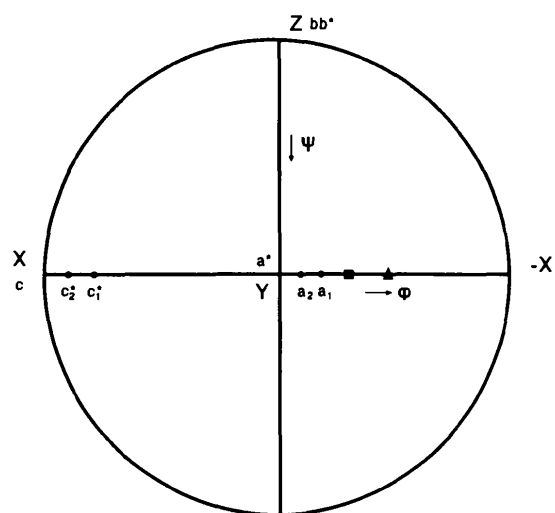

Fig. 1. Self-rotation function ($\kappa = 180.0°$ section) for two monoclinic crystal forms. The crystallographic c axis is along X, a^* along Y, and b^* along Z, where XYZ are the right-handed orthogonal reference axes in *MERLOT* (Fitzgerald, 1988). ψ is positive from Z to Y and φ is positive from Y to $-X$ in the XY plane. (▲) and (■) are the positions of two density peaks at $\varphi = 22.0$, $\psi = 90.0$ and $\varphi = 52.5$, $\psi = 90.0°$ respectively.

average ratio $I/\sigma(I) = 24.6$ at this resolution. The self-rotation function calculated using data between 8 and 5 Å resolution with a cut-off radius of 29.0 Å displayed a peak of 7.1 standard deviations above background at $\varphi = 52.5$, $\psi = 90.0$ and $\kappa = 180.0°$ indicating the presence of two molecules per asymmetric unit related by a non-crystallographic twofold axis (Fig. 1). The new monoclinic crystal form was used in screening for heavy-atom derivatives and molecular-replacement studies. The crystal data and unit-cell parameters are listed in Table 1.

Heavy-atom-derivative preparation

A highly concentrated solution of potassium platinum nitrite, a compound found to bind isomorphously to porcine aldose reductase crystals (El-Kabbani *et al.*, 1991) was added directly to the protein droplet containing the aldehyde reductase crystals. The concentration of the heavy atom in the drop was approximately 5 mM and the soaking time 8 d. Final derivative merged data (resolution 3.5 Å) had 8568 out of 8588 possible unique reflections with 8321 reflections measured more than once. The value for R_{sym} is 10.2% and the average ratio $I/\sigma(I) = 31.6$ at this resolution. The mean fractional difference between the native and derivative data sets is equal to 19.6% for data between 12 and 4 Å resolutions. One platinum site was located from a three-dimensional isomorphous difference Patterson map using 5559 reflections between 12 and 4 Å resolution $[I > 3\sigma(I)]$. The positional parameters, isotropic temperature factor and occupancy for the platinum site were refined by lack-of-closure-error minimization
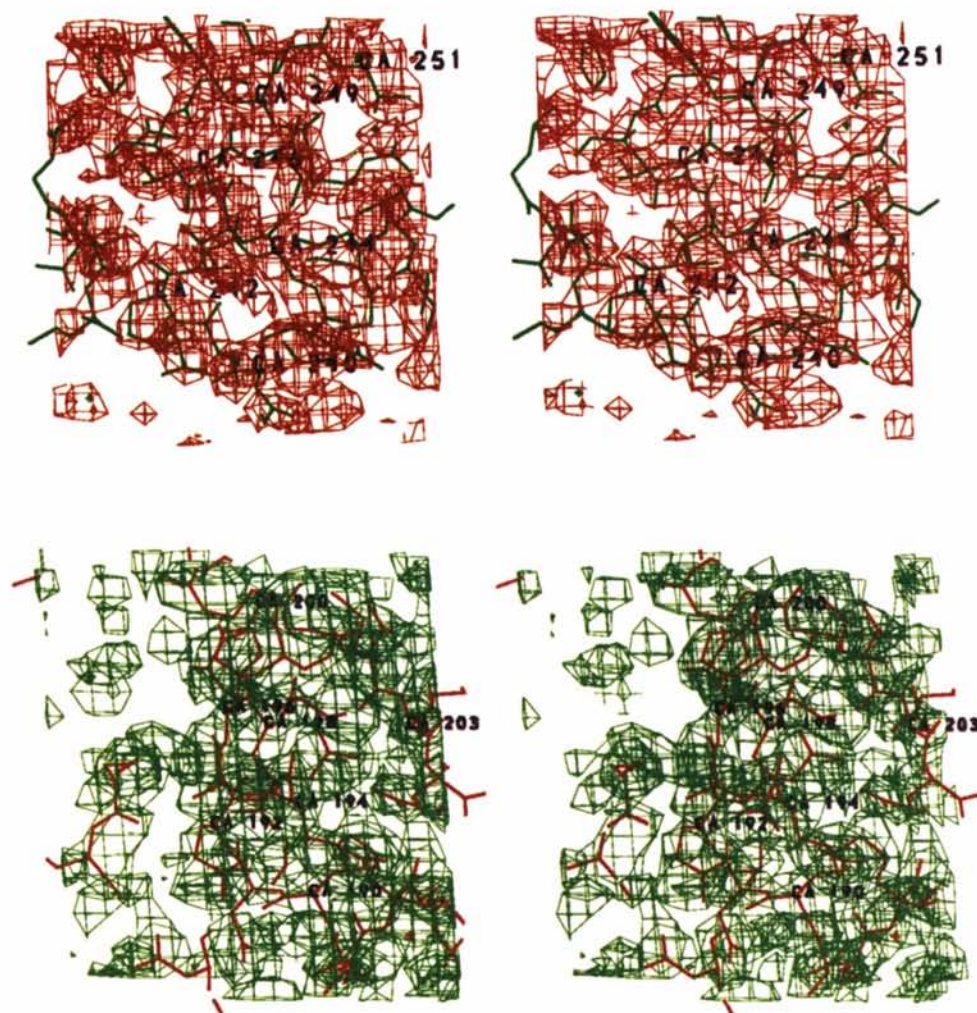

Fig. 2. Stereo drawings showing helix 7 (top) and helix 6 (bottom) of the first and second monoclinic crystal forms, respectively, with superimposed electron-density contour surfaces. The 2.8 Å resolution $(2F_o - F_c)$ electron-density maps were prepared after one round of simulated-annealing refinement (Brünger, Kuriyan & Karplus, 1987; Brünger, Krukowski & Erickson, 1990). Selected Cα atoms from the two helices are labeled.

Table 1. *Porcine aldehyde reductase crystal parameters*

	Monoclinic		Hexagonal
a (Å)	56.2	92.4	166.0
b (Å)	98.1	62.1	166.0
c (Å)	73.2	59.0	66.0
α ( )	90.0	90.0	90.0
β ( )	112.5	94.6	90.0
γ ( )	90.0	90.0	120.0
Space group	$P2_1$	$P2_1$	$P622, P6_122, P6_522,$ $P6_322, P6_422$ or $P6_322$
Molecules per unit cell	4	4	12
V_m (Å Da $^{-1}$)	2.47	2.22	3.45
Solvent content (%)	51	45	64

Table 2. *Heavy-atom-derivative phasing statistics*

Resolution range (Å)	12 3.5
Isomorphous differences (No.)	7525
F_H residual (r.m.s.)	1.37
R_{Cullis}*	0.61
Mean figure of merit	0.35

$$* R_{Cullis} = \sum ||F_{PH} \pm F_P \cdot F_H| \sum |F_{PH} - F_P.$$

Table 3. *Refined rotational and translational parameters*

	α	β	γ	Δx	Δy	Δz
Molecule A	98.64	69.70	171.20	0.724	0.210	0.766
Molecule B	6.20	108.40	354.80	0.417	0.002	0.407

(Blundell & Johnson, 1976). A second platinum site was located from a residual-difference Fourier map. The heavy-atom derivative phasing statistics are given in Table 2. The electron-density map calculated using the observed native amplitudes and phases from the platinum sites revealed a clear demarkation of the solvent boundary in the unit cell.

Results and discussion

Molecular-replacement studies

Although the primary sequence of porcine aldehyde reductase is not yet available, comparison of the sequence of human aldehyde reductase with porcine aldose reductase shows 49% identity (Bohren *et al.*, 1989; Kubiseski, Green & Flynn, 1992). This laboratory obtained the three-dimensional structure of porcine aldose reductase complexed with ADP at 3.2 Å resolution by multiple isomorphous replacement methods (unpublished results). High-resolution structures of porcine aldose reductase (2.5 Å) and human aldose reductase (1.65 Å) complexed with ADPRP and NADPH respectively, have been determined recently (Rondeau *et al.*, 1992; Wilson *et al.*, 1992). A concensus primary sequence using the human aldehyde reductase and porcine aldose reductase sequences has been built and used with the porcine aldose reductase structure as a starting model for molecular-replacement studies. The search model (consisting of a single polypeptide chain of 313 amino acids) folds into an eight-stranded parallel α/β barrel. This $(\alpha/\beta)_8$ barrel was first observed for triose phosphate isomerase (Banner *et al.*, 1975) and is referred as the 'TIM-barrel'. The symmetrical appearance of the model structure is diminished by the presence of two

short antiparallel β-strands at the N-terminus (residues 2–5 and 9–12) that are connected by a tight turn and close off the bottom of the barrel. Loops A, B (at the C-terminal ends of β-strands 4 and 7) and C (at the C-terminus) partially cover the top of the barrel. Two extra pieces of α-helix are present. The first between strand 7 and helix 7 (residues 230–239) and the second between helix 8 and loop C (residues 281–288). The rotation function, calculated by the Crowther algorithm (Crowther, 1972), used several trials at different resolution shells and radii of integration. A cross-rotation function displayed two consistent peaks which are related to each other by a non-crystallographic twofold symmetry at $\varphi = 52.5$, $\psi = 90.0$ and $\kappa = 180.0°$, similar to that obtained from the self-rotation function. By using data between 10 and 4 Å resolution with a cut-off radius of 23.0 Å, two peaks of 6.2 and 5.8 standard deviations above background were displayed with no other peaks > 70% of the first peak found.

The two crystallographically independent molecules in the unit cell were rotated into their orientations and maps of intermolecular vectors calculated (Crowther & Blow, 1967) using data between 8 and 5 Å resolution. This translation search revealed a single vector separating the two molecules from which the molecular translations for the two molecules and their position in the crystallographic asymmetric unit were calculated. After refinement of the rotational and translational parameters, the initial R factor equaled 0.49; 15 cycles of refinement using the 2088 reflections between 12 and 5 Å resolution produced an R factor equaling 0.45 (where $R = \sum |F_o - F_c|/\sum |F_o|$, F_o is the observed and F_c is the calculated structure factor). The final rotational and translational parameters are listed in Table 3 where α, β, γ are the rotation Euler angles and Δx, Δy, Δz are the translations in fractional coordinates. These calculations were performed by using the *MERLOT* program package (Fitzgerald, 1988).

The molecular-replacement model (3934 non-H atoms for the two molecules) had an initial R factor of 0.43 at 3.0 Å resolution (Tronrud, Ten Eyck & Matthews, 1987). There were 12 285 observed reflections out of 13 645 possible unique reflections with a $4.0\sigma F$ cutoff for data between 12 and 3.0 Å resolution. Eight cycles of rigid-body refinement produced an R factor of 0.40. Phases from the molecular-replacement model were used to cross phase a difference map for the heavy-atom derivative. The

major heavy-atom site was the only peak present on the cross-phased difference map. The molecular-replacement and the single isomorphous replacement (SIR) phases (anomalous signal was not used in SIR phasing) were combined and a 3.0 Å electron-density map was calculated by using coefficients that suppress model bias (Read, 1986). The electron-density map was displayed on an Evans & Sutherland PS330 computer graphics system by using the *FRODO* software (Jones, 1978). Electron densities corresponding to side chains of amino-acid residues which were not included in the search model were evident

on this map. After one round of model refitting and simulated-annealing refinement using the slow-cooling protocol of the *X-PLOR* package (Brünger, Kuriyan & Karplus, 1987; Brünger, Krukowski & Erickson, 1990), the *R* factor dropped to 0.25 at 8–2.8 Å resolution (13 427 reflections) with root-mean-square (r.m.s.) deviation of bond lengths and bond angles from ideality of 0.022 Å and 2.4°, respectively. During the refinement, the non-crystallographic twofold axis was used as a constraint to improve parameter to observation ratios at this resolution. A sample of the electron-density map
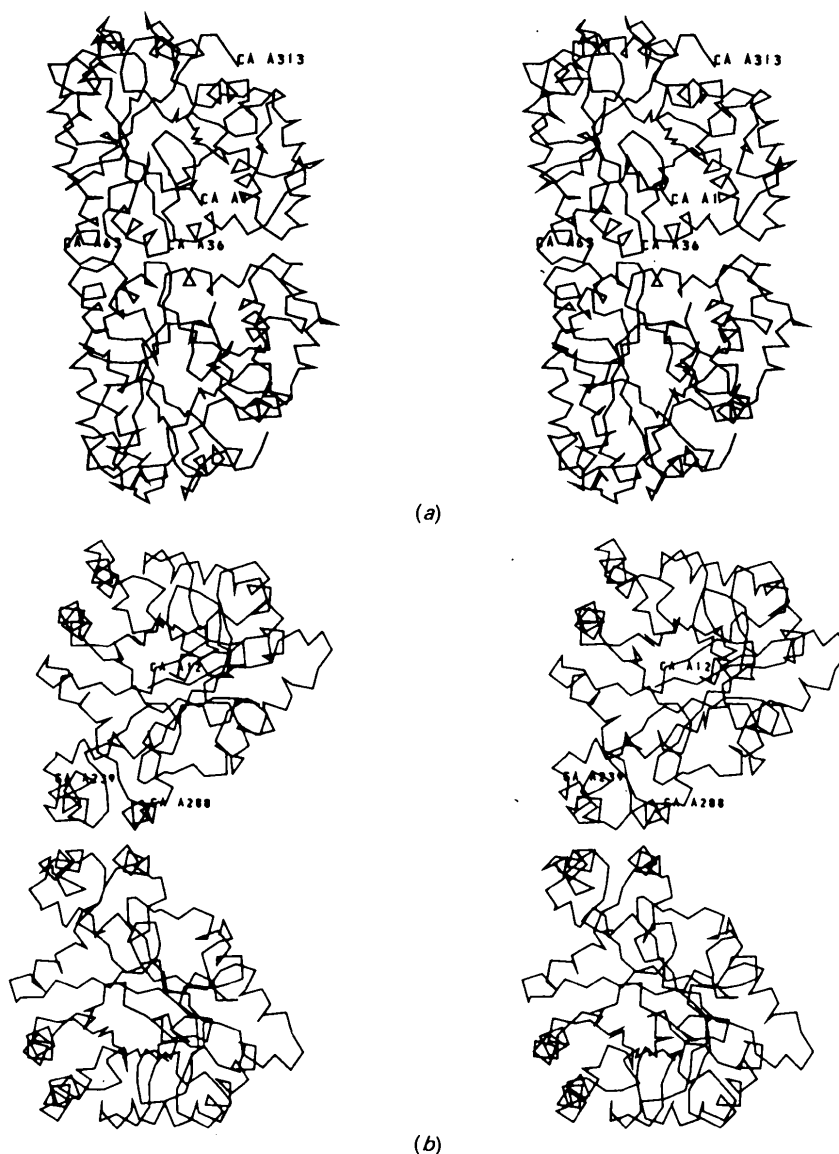

(a)

(b)

Fig. 3. Stereo images of the two crystallographically independent molecules (A and B) for the two monoclinic crystal forms. Selected Cα atoms from molecule A (top) are labeled. (a) Molecules A and B of the first monoclinic crystal form viewed down the crystallographic a axis with the non-crystallographic twofold axis horizontally oriented. (b) View of molecules A and B of the second monoclinic crystal form down the crystallographic b axis with the non-crystallographic axis horizontally oriented.

Table 4. *Refined rotational and translational parameters for the first monoclinic crystal form*

	α	β	γ	Δx	Δy	Δz
Molecule *A*	34.40	139.04	195.75	0.444	0.500	0.490
Molecule *B*	10.40	40.76	15.70	0.047	0.000	0.490

is shown in Fig. 2. Amino-acid residues that are missing from the current model will be substituted and the refinement extended to high resolution as the amino-acid sequence becomes available.

Atomic coordinates for molecule *B* were used as the search model in molecular-replacement studies for the first monoclinic crystal form. When a cross-rotation function was calculated using data between 10 and 4 Å resolution with a cut-off radius of 23 Å two peaks of 6.1 and 5.7 standard deviations above background were displayed which are related to each other by a non-crystallographic twofold symmetry at $\varphi = 22.5$, $\psi = 90.0$ and $\kappa = 180.0$ (similar to that obtained from the self-rotation function). There were no other peaks > 70% of the first peak found. Maps of intermolecular vectors were calculated using data between 8 and 4 Å resolution, and translation distances for the two molecules from their initial positions calculated. The rotational and translational parameters were refined to determine a local minimum in the *R* factor. The starting *R* factor equalled 0.45 and decreased to 0.43 after ten cycles using the 2624 reflections between 12 and 5 Å resolution (Fitzgerald, 1988). The refined rotational and translational parameters are listed in Table 4.

The initial *R* factor for the moelcular-replacement model equalled 0.43 using 12 757 observed reflections out of 17 945 possible unique reflections with a $4.0\sigma F$ cut-off for data between 8 and 2.8 Å resolution. Nine cycles of rigid-body refinement decreased the *R* factor to 0.40 (Tronrud *et al.*, 1987). When rigid-body refinement was followed by simulated-annealing refinement (Brünger, Kuriyan & Karplus, 1987; Brünger, Krukowski & Erickson, 1990) using the non-crystallographic twofold axis as a constraint, the *R* factor dropped to 0.23 for data between 8 and 2.8 Å resolution with r.m.s. deviations from ideal bond lengths and bond angles equal to 0.024 Å and 2.7°, respectively. A section of the 2.8 Å resolution electron-density map is shown in Fig. 2. We do not see electron density which may correspond to endogenously bound NADPH.

The relative orientations of the two crystallographically independent molecules (*A* and *B*) for the two monoclinic crystal forms are shown in Fig. 3. A non-crystallographic twofold axis in the *ac* plane perpendicular to the *b* axis relates the two molecules. The intermolecular contacts between molecules *A* and *B* of the first monoclinic crystal form are formed by residues connecting helix 1 and strand 2, and helix

2 and strand 3 of the α/β barrel from molecule *A* and their symmetry-related residues from molecule *B* (Fig. 3a). The interface around the non-crystallographic twofold axis for the second monoclinic crystal form is held together by hydrophobic and polar residues from the extra two pieces of helix (residues 230–239 and 281–288) that are not part of the α/β barrel (Fig. 3b). A second non-crystallographic twofold axis is generated for each crystal form by applying crystallographic symmetry operations on molecules *A* and *B*. This non-crystallographic twofold axis relates each molecule to the symmetry-generated molecule of the other. The non-specific interactions between molecules *A* and *B* at the interface around the non-crystallographic twofold axis which exists in the two crystal forms may be present because of the monomeric nature of the enzyme in solution (Flynn, 1982). The detailed intermolecular interactions should be available after the sequence of the pig kidney aldehyde reductase has been completed and the remaining amino-acid residues positioned based on corresponding electron density.

Recently obtained high-resolution crystals of human aldehyde reductase led to a rotation–translation function solution using the structure of pig kidney aldehyde reductase as a search model (unpublished results). The structures of porcine and human aldehyde and porcine and human aldose reductases will be compared. The detailed information learnt from these three-dimensional structures will be useful in the design of active-site directed inhibitors which may prevent or reduce many of the complications associated with diabetes.

References

BANNER, D. W., BLOOMER, A. C., PETSKO, G. A., PHILLIPS, D. C., POGSON, C. I., WILSON, I. A., CORRAN, P. H., FURTH, A. J., MILMAN, J. D., OFFORD, R. E., PRIDDLE, J. E. & WALEY, S. G. (1975). *Nature (London)*, **255**, 609–614.

BLUNDELL, T. L. & JOHNSON, L. N. (1976). *Protein Crystallography*, pp. 333–336. New York: Academic Press.

BOHREN, K. M., BULLOCK, B., WERMUTH, B. & GABBAY, K. H. (1989). *J. Biol. Chem.* **264**, 9547–9551.

BRÜNGER, A. T., KRUKOWSKI, A. & ERICKSON, J. (1990). *Acta Cryst.* A**46**, 585–593.

BRÜNGER, A. T., KURIYAN, J. & KARPLUS, M. (1987). *Science*, **35**, 458–460.

CROMLISH, J. A. & FLYNN, T. J. (1983). *J. Biol. Chem.* **258**, 3583–3586.

CROWTHER, R. A. (1972). *Molecular Replacement Method*, edited by M. G. ROSSMANN, pp. 173–178. New York: Gordon and Breach.

CROWTHER, R. A. & BLOW, D. M. (1967). *Acta Cryst.* **23**, 544–548.

EL-KABBANI, O., NARAYANA, S. V. L., BABU, Y. S., MOORE, K. M., FLYNN, T. G., PETRASH, J. M., WESTBROOK, E. M., DELUCAS, L. J. & BUGG, C. E. (1991). *J. Mol. Biol.* **218**, 695–698.

FITZGERALD, P. M. D. (1988). *J. Appl. Cryst.* **21**, 273–278.

FLYNN, T. G. (1982). *Biochem. Pharmacol.* **31**, 2705–2712.

HOWARD, A. J., GILLILAND, G. L., FINZEL, B. C., POULOS, T. L., OHLENDORF, D. H. & SALEMME, F. R. (1987). *J. Appl. Cryst.* **20**, 382–387.

JONES, A. T. (1978). *J. Appl. Cryst.* **11**, 268–272.

KINOSHITA, J. H. & NISHIMURA, C. (1988). *Diabetes Metab. Rev.* **4**, 323–337.

KUBISESKI, T. J., GREEN, N. C. & FLYNN, T. G. (1992). *Enzymology and Molecular Biology of Carbonyl Metabolism*, edited by H. WEINER, T. J. FLYNN & D. W. CRABB, p. 4. New York: Plenum Press.

KUBISESKI, T. J., HYNDMAN, D. J., MORJANA, N. A. & FLYNN, T. G. (1992). *J. Biol. Chem.* **267**, 6510–6517.

MCPHERSON, A. (1985). *Methods Enzymol.* **114**, 112–120.

MARKUS, H. B., RADUCHA, M. & HARRIS, H. (1983). *Biochem. Med.* **29**, 31–45.

READ, R. (1986). *Acta Cryst.* **A42**, 140–149.

RONDEAU, J.-M., TÉTE-FAVIER, F., PODJARNY, A., REYMANN, J.-M., BARTH, P., BIELLMANN, J.-F. & MORAS, D. (1992). *Nature (London)*, **355**, 469–472.

STRIBLING, D., MIRLEES, D. J., HARRISON, H. E. & EARL, D. C. N. (1986). *Metabolism*, **34**, 336–344.

TRONRUD, D. E., TEN EYCK, L. F. & MATTHEWS, B. W. (1987). *Acta Cryst.* **A43**, 489–501.

WILSON, D., BOHREN, K. M., GABBAY, K. H. & QUIOCHO, F. A. (1992). *Science*, **2257**, 81–84.